Originally published in *Proceedings of the Fifth International Workshop on Compressible Turbulent Mixing*, ed. R. Young, J. Glimm & B. Boston.
ISBN 9810229100, World Scientific (1996).

Turbulent Mixing Modeling and Simulation

D. Besnard, F. Ducros, Ph. Loreaux,
S. Mimouni, and A. Vasseur

Centre d'études de Limeil-Valenton
94195 Villeneuve-St-Georges CEDEX France

Abstract. This paper covers modeling efforts at the CEL-V Applied Maths Dept. Several items are discussed, including spectral transport modeling of turbulent mixtures, LES and DNS simulations of instability induced mixing, and analysis of geometrical patterns in such flows.

1 Introduction

ICF related flows are highly non stationary and, when turbulent, cannot be described with models that rely on an spectral equilibrium assumption. The spectral transport model developed by Besnard and al. [9] was generalized to multimaterial flows to address this problem. Part 1 of this paper emphasizes some of the features of this new model.

LES modeling is a promising complement to transport models for simulating mixing processes. The sensitivity of results to the choice of numerical schemes and models was explored. A massively parallel version of a 3D Navier-Stokes solver was developed, to which was added a LES capability. Some early results are discussed in Part 2.

Very little is known about the geometrical structure of mix layers. Based on numerical simulations, a model was developed that gives the probability distribution function of the materials in a layer induced by Rayleigh-Taylor instability. From this pdf, average variables may be deduced; we concentrate here on the calculation of an effective opacity in the mix region.

2 Spectral transport model for turbulence

Classical mixing turbulence models are based upon spectral equilibrium assumption, leading to a small number of equations in the flow description. But these models are not well suited for non stationary flows. Consequently, models giving information on the turbulence spectrum itself have to be developed. The case of the incompressible turbulence has been studied in a collaboration with the LANL T3 group. We recall

the BHRZ equations system which depends on time t, space variable x, and spectral variable k :

$$\begin{aligned}\frac{\partial E}{\partial t}+u_n\frac{\partial E}{\partial x_n} = & \ \nu\left(-2k^2+\tfrac{1}{2}\nabla^2\right)E+c_D\tfrac{\partial}{\partial x_n}\left\{\nu_T\tfrac{\partial E}{\partial x_n}\right\}\\ & -c_1\tfrac{\partial}{\partial k}\left\{k^2\sqrt{kE}E\right\}+c_2\tfrac{\partial}{\partial k}\left\{k^3\sqrt{kE}\tfrac{\partial E}{\partial k}\right\}-2\tfrac{\partial u_n}{\partial x_m}\tilde{E}_{nm},\end{aligned}$$

$$\begin{aligned}\frac{\partial \tilde{E}_{ij}}{\partial t}+u_n\frac{\partial \tilde{E}_{ij}}{\partial x_n} = & \ \nu\left(-2k^2+\tfrac{1}{2}\nabla^2\right)\tilde{E}_{ij}+c_D\tfrac{\partial}{\partial x_n}\left\{\nu_T\tfrac{\partial \tilde{E}_{ij}}{\partial x_n}\right\}-c_1\tfrac{\partial}{\partial k}\left\{k^2\sqrt{kE}\tilde{E}_{ij}\right\}\\ & +c_2\tfrac{\partial}{\partial k}\left\{k^3\sqrt{kE}\tfrac{\partial \tilde{E}_{ij}}{\partial k}\right\}-\tfrac{1}{3}(1-c_B)\left(\tfrac{\partial u_i}{\partial x_j}+\tfrac{\partial u_j}{\partial x_i}\right)E\\ & -(1-c_B)\left\{\tfrac{\partial u_i}{\partial x_n}\tilde{E}_{nj}+\tfrac{\partial u_j}{\partial x_n}\tilde{E}_{in}-\tfrac{2}{3}\delta_{ij}\tfrac{\partial u_m}{\partial x_n}\tilde{E}_{nm}\right\},\end{aligned}$$

with $E_{ij}=\frac{1}{3}E\delta_{ij}+\tilde{E}_{ij}$ and $E_{ij}=\int\overline{u_i'(x-\frac{r}{2})u_j'(x+\frac{r}{2})}e^{-ir.k}dr$ and u' the fluctuating part of U.

First, we have shown some results of coherence of this system of equations, then extended it to the compressible turbulence modeling at variable density and for small turbulent Mach numbers.

1: E represents an energy density, and then must stay positive. We have shown that, without the coupling term $-2\frac{\partial u_n}{\partial x_m}\tilde{E}_{nm}$ in the first equation, this property is confirmed.

We now consider the coupling term $-2\frac{\partial u_n}{\partial x_m}\tilde{E}_{nm}$ which models :

$$F_{nm}(x,k)=\int e^{-ik.r}\frac{\partial u_n}{\partial x_m}(x+\frac{r}{2})R_{nm}(x+\frac{r}{2},x-\frac{r}{2})dr,$$

where $R_{nm}(x_1,x_2)=\overline{u_n'(x_1)u_m'(x_2)}$.

Using Taylor's theorem for $\frac{\partial u_n}{\partial x_m}$ we formally have :

$$F_{nm}(x,k)=\exp\left(\frac{1}{2}i\frac{\partial}{\partial x_l}(u)\frac{\partial}{\partial k_l}\right)\frac{\partial u_n}{\partial x_m}(x)E_{nm}(x,k).$$

Remark : the coupling term follows this approximation at first order.

Then, we have shown that, if the turbulence is located in a bounded domain and if u is analytic, we have the following estimate :

$$\forall x,k\ :\left|F_{nm}(x,k)-\sum_{m=0}^{N}\frac{1}{m!}\left(\frac{1}{2}i\frac{\partial}{\partial x_l}(u)\frac{\partial}{\partial k_l}\right)^m\left(\frac{\partial u_n}{\partial x_m}E_{nm}(x,k)\right)\right|\leq 8\epsilon\mathcal{E}(t),$$

where $\mathcal{E}(t)$ is the total turbulent energy : $\mathcal{E}(t)=\int_x\int_k E(x,k,t)dx\,dk$ and ϵ is the approximation error of $\frac{\partial u_n}{\partial x_m}$ at order N.

2: We derived a model for compressible flows at variable density which is a generalization of the previous one. We proved that $div\, u' = 0$, if a small turbulent Mach number is assumed. This estimation has been used, but no constraint on the main flow has been assumed. We considered evolution equations for the Fourier transforms of the following terms :

$$
\begin{aligned}
&R_{ij}(x_1;x_2) = \overline{\tfrac{\rho(x_1)+\rho(x_2)}{2} u_i''(x_1) u_j''(x_2)}, \quad && A_{i\alpha}(x_1;x_2) = \overline{u_i''(x_1)\rho(x_2)C_\alpha''(x_2)},\\
&a_i(x_1;x_2) = \overline{u_i''(x_1)\rho(x_1)\nu(x_2)}, && a_\alpha(x_1;x_2) = \overline{\nu(x_2)\rho(x_1)C_\alpha''(x_1)},\\
&b\,(x_1;x_2) = -\overline{\rho'(x_1)\nu'(x_2)}.
\end{aligned}
$$

For instance, comparing with the incompressible case, the equation of $R_{ij}(x_1, x_2)$ is given by :

$$
\begin{aligned}
\frac{\partial R_{ij}(x,k)}{\partial t} = {} & \frac{\partial}{\partial k}\left\{k\frac{\partial \tilde{u}_n(x)}{\partial x_l} M_{ij}^{nl}(x,k)\right\} - \frac{\partial \tilde{u}(x) R_{ij}(x,k)}{\partial x_n}\\
& - \left(1 - C_B\left[1+\frac{b(x)}{2}\right]\right)\left(\frac{\partial \tilde{u}_i(x)}{\partial x_n} R_{nj}(x,k) + \frac{\partial \tilde{u}_j(x)}{\partial x_n} R_{in}(x,k)\right)\\
& - \frac{2}{3} C_B\left[1+\frac{b(x)}{2}\right]\delta_{ij}\frac{\partial \tilde{u}_m(x)}{\partial x_n} R_{nn}(x,k) + C_{RH}\beta_{RH}(k)\bar{D}k^2 R_{ij}(x,k)\\
& - C_{R2}\frac{\partial}{\partial k}\left\{[1+C_{RB}\beta_{RB}]\left[\tfrac{1}{\bar{\rho}(x)}\int_0^k q^2 R_{nn}(x,q)dq\right]^{\frac{1}{2}}\left[\tfrac{C_{R_1}}{C_{R_2}} k R_{ij}(x,k) - k^2\tfrac{\partial R_{ij}(x,k)}{\partial k}\right]\right\}\\
& + \left\{C_{RP1}\beta_{RP1}(k)\bar{\rho}(x)k^2\sqrt{a_n(x,k)a_n(x,k)}\right\}\{a_i(x,k)a_j(x) + a_j(x,k)a_i(x)\}\\
& + \left\{C_{RP2}\beta_{RP2}(k)\bar{\rho}(x)\left[\tfrac{1}{\bar{\rho}(x)}\int_0^k q^2 R_{nn}(x,q)dq\right]^{\frac{1}{2}}\right\}\{a_i(x,k)a_j(x) + a_j(x,k)a_i(x)\}\\
& - C_{RTI}\left[\tfrac{1}{\bar{\rho}(x)}\int_0^k q^2 R_{nn}(x,q)dq\right]^{\frac{1}{2}}\left\{R_{ij}(x,k) - \frac{1}{3}\delta_{ij}R_{nn}(x,k)\right\}\\
& + C_D\frac{\partial}{\partial x_n}\left\{\nu_T\frac{\partial R_{ij}(x,k)}{\partial x_n}\right\} - \frac{\partial \bar{P}(x)}{\partial x_j}a_i(x,k) - \frac{\partial \bar{P}(x)}{\partial x_i}a_j(x,k)\\
& - \tfrac{2+b(x)}{\bar{\rho}(x)}\left(\tfrac{\partial R_{nn}(x)}{\partial x_n} + \tfrac{\partial \bar{P}(x)}{\partial x_n} - \mu\tfrac{\partial \bar{\tau}_{nm}(x)}{\partial x_n}\right)[(q_1^a + q_2^a)\,[a_i(x,k) + a_j(x,k)] + 2q_2^a\delta_{ij}a_m(x,k)]\\
& + \mu a_i(x,k)\left[D_j^2[\tilde{u}(x) + \frac{1}{2}a(x)]\right] + \mu a_j(x,k)\left[D_i^2[\tilde{u}(x) + \frac{1}{2}a(x)]\right]\\
& + \mu\bar{\nu}(x)\left[\frac{1}{2}\Delta R_{ij}(x,k) - 2k^2 R_{ij}(x,k)\right] - \frac{\mu}{2}\Delta a_i a_j(x,k) + 2\mu k^2 a_i a_j(x,k).
\end{aligned}
$$

Current efforts pertain to the reduction to one-point equations such as "$K-\epsilon$".

Figure 1: Section at $x_2 = L_{x_2}/2$ for $t = 5.75ms$ (left) and $t = 6.83ms$ (right) for a $(2,2)$ order calculation; the denser fluid (left) penetrates the less dense one by developing the well-known mushroom shape, secondary instabilities are observed at the interface.

3 Three-dimensional simulations of Rayleigh-Taylor instability

3.1 Physical issues and numerical choices

We briefly recall the importance of Rayleigh-Taylor instability in inertial confinement fusion (I.C.F.) experiments and the crucial issue of its numerical simulation. From a phenomenological point of view, Rayleigh-Taylor instabilities develop on shell interfaces of targets which symmetry is thus degraded.

Their simulations require numerical methods, robust enough to treat sharp gradients (*e.g.* discontinuity in concentration) and compressible effects, and able to let small scales develop freely during transition to turbulence.

Towards a L.E.S. formulation of the problem: as shown by [7], the projection of the governing equations on a grid acts as a convolution by a sharp cut-off low pass filter (noted $^-$). Density-weighted filtered variables are defined in the same manner ($\tilde{\phi} = \overline{\rho\phi}/\overline{\phi}$), leading to the following low pass filtered complete Navier-Stokes equations in their conservative form:

$$\frac{\partial \overline{U}}{\partial t} + \frac{\partial(\overline{F}_1 - \overline{D}_1)}{\partial x_1} + \frac{\partial(\overline{F}_2 - \overline{D}_2)}{\partial x_2} + \frac{\partial(\overline{F}_3 - \overline{D}_3)}{\partial x_3} = \bar{\rho} g_i,$$

with

$$\overline{U} = {}^T(\overline{\rho}, \overline{\rho}\widetilde{u_1}, \overline{\rho}\widetilde{u_2}, \overline{\rho}\widetilde{u_3}, \overline{\rho}\widetilde{e}, \overline{\rho}\widetilde{c_n}),$$

where

$$\overline{F_i} = \begin{pmatrix} \overline{\rho}\widetilde{u_i} \\ (\overline{p} - \frac{1}{3}\mathcal{T}_{ll})\ \delta_{i1} + \overline{\rho}\widetilde{u_i}\widetilde{u_1} \\ (\overline{p} - \frac{1}{3}\mathcal{T}_{ll})\ \delta_{i2} + \overline{\rho}\widetilde{u_i}\widetilde{u_2} \\ (\overline{p} - \frac{1}{3}\mathcal{T}_{ll})\ \delta_{i3} + \overline{\rho}\widetilde{u_i}\widetilde{u_3} \\ (\bar{\rho}\tilde{e} + (\bar{p} - \frac{1}{3}\mathcal{T}_{ll}))\tilde{u}_i \\ \overline{\rho}\tilde{c}_n\widetilde{u_i} \end{pmatrix}, \overline{D_i} = \begin{pmatrix} 0 \\ (\frac{\mu}{Re} + \bar{\rho}\nu_t)\tilde{S}_{i1} \\ (\frac{\mu}{Re} + \bar{\rho}\nu_t)\tilde{S}_{i2} \\ (\frac{\mu}{Re} + \bar{\rho}\nu_t)\tilde{S}_{i3} \\ \frac{\mu}{Re}\tilde{u}_i\tilde{S}_{ij} + (\frac{\gamma}{RePr}\mu + \frac{\bar{\rho}\nu_t}{Pr_t})(\frac{\partial\tilde{\epsilon}}{\partial x_i}) \\ (\frac{\mu}{ReSci} + \frac{\bar{\rho}\nu_t}{Sci_t})(\frac{\partial\tilde{c}_n}{\partial x_i}) \end{pmatrix}.$$

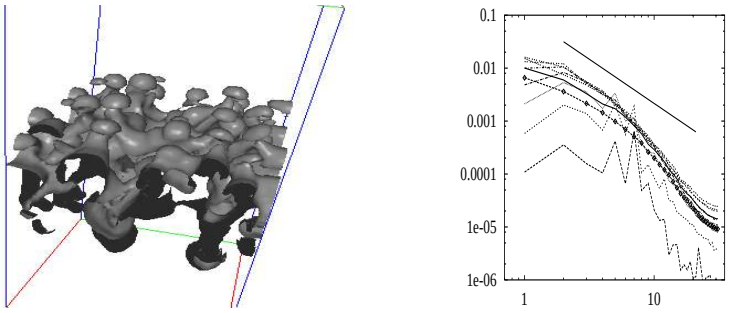

Figure 2: Isosurface $c_1 = 0.6$ for $t = 3.84ms$ (left) and mono-dimensional energy spectrum of c_1 on x_1 for $t = 1.44, 3.26, 4.91, 6.46, 8.00, 9.52, 1.10, 1.27, 1.43, 1.60$ ms (the eventual curve is marked with points) plus a $k^{-5/3}$ slope of reference (right).

The gas mixture obeys a simplified filtered stiffened gas approximation law:

$$\tilde{\epsilon} = \frac{\overline{p} + \overline{\gamma}\ \overline{p}_0}{(\overline{\gamma} - 1)\bar{\rho}}.$$

$\mathcal{T}$ is the subgrid scale tensor, $\mathcal{T}_{ij} = -\overline{\rho u_i u_j} - \bar{\rho}\tilde{u}_i\tilde{u}_j$ and $S_{ij} = \frac{1}{2}(\frac{\partial \tilde{u}_i}{\partial x_j} - \frac{\partial \tilde{u}_j}{\partial x_i}) - \frac{2}{3}\vec{\nabla}\vec{\tilde{u}}\ \delta_{ij}$. F_i and D_i are the fluxes and the diffusivity tensors in the i direction; $\bar{\rho}$, $\tilde{u}_i$, $\tilde{e}$, $\tilde{\epsilon}$, $\tilde{c}_n$, g_i are respectively the resolved density, velocity, total and internal energy, concentration of the species and the gravity force; γ, μ, Re, Pr, Sci are the the specific heat ratio, the molecular viscosity, the Reynolds, Prandtl and Schmidt numbers. We can take into account the action of non-resolved scales on the resolved motion by means of a sub-grid scale model based on the introduction of a turbulent viscosity ν_t, diffusivity of heat ν_t/Pr_t and species ν_t/Sci_t (see [5] for details). This set of equations is resolved by a code based on Mc-Cormack-type schemes [6] of order $(2, 2)$ or $(2, 4)$ in time and space, in combination with a flux limiter [6] adapted to multi-species transport to get a TVD scheme and implemented on CM5 [6]. Diffusive terms are treated through second order centered differences.

3.2 Results

Let us note x_3 the direction where the gravity points; x_1 and x_2 are the directions perpendicular to x_3. At $t = 0$, the density follows an exponential distribution along x_3: its values vary from $\rho_1 = 0.1694kg/m^3$ to $\rho_2 = 1.225kg/m^3$ from one side to another of an interface $Z(x_1, x_2)$. We set $\gamma_1 = 1.67$, $\gamma_2 = 1.4$; the pressure follows the hydrostatic equilibrium, imposed by the gravity $g = 2.5\ 10^5 m/s^2$. Rigid wall boundary conditions are applied at each face of the domain which dimensions are $L_{x_1} = L_{x_2} = 1/2L_{x_3} = 1.75mm$ for a resolution of $64 \times 64 \times 128$. The Reynolds number is set to 10^4, which corresponds to almost non viscous flow ($\mu \approx 10^{-7} Pl$).

• Single-mode case.
We performed two simulations for $(2,2)$ and $(2,4)$ order schemes, without any turbulent viscosity because turbulence is weak in this case. For both simulations we observe the development of the instability up to the impact on the wall (fig. 1).

Linear stability studies show a time evolution of the penetration depth $a(t)$ of the form $a_0 e^{nt}$ with $n = 824s^{-1}$ for our set of parameters [8]. Our numerical estimation gives $n \approx 731s^{-1}$ and $n \approx 802s^{-1}$ for the $(2,2)$ and $(2,4)$ calculations respectively.

• Multi-mode case.
Transition to turbulence is so abrupt in this case that the action of non-resolved scales seems no more negligible; ν_t is given by the "filtered structure function model" [7], Pr_t and Sci_t are taken equal to 0.6 on the basis of passive scalar turbulent diffusion.

An isosurface of concentration (fig. 2, left) shows the penetration of "bubbles" of the less dense fluid (towards the top) and "spikes" of the denser one (towards the bottom): this view is reminiscent, on one hand of many experiments, and on the other hand of Youngs' numerical results [8]. Moreover, a global evaluation of $\alpha = a(t)/At\ g\ t^2$ gives approximately $\alpha \approx 0.09$, which compares well with Youngs' estimation. After the filling up of all the spectrum due to transition to turbulence (fig 2, right), an self-similar decay of the turbulent kinetic energy is exhibited from $t \approx 6.46ms$ to the end of the calculation, that is before any interaction with the walls. The slope of the spectrum is seen to match pretty well a $k^{-5/3}$ behavior.

3.3 Discussions and conclusions

Even if the main features of Rayleigh-Taylor instability are captured by the simulation, many questions remain open, among them the sensitivity to initial conditions. Numerically speaking, only weak differences are observed between $(2,2)$ and $(2,4)$ order calculations. Moreover, the real part played by the flux limiter and the subgrid model in the global result is not clear. Eventually, we want to stress the necessity of further diagnostics to get more precise information about the transition process (Fourier or wavelet analysis for example).

4 Patterns in instability analysis - induced mix layers

4.1 Introduction

The passive convection of Lagrangian points by a 2D compressible two-fluids flow is investigated numerically on a massively parallel computer. The numerical simulation are devoted to the Rayleigh-Taylor instability. We compute the fractal dimension of a set of tracer particles located along the interface between the two fluids. A first result is that this dimension reaches a stationary value. Then this result is used to determine the effective opacity of the mixture.

In the second part we study the morphology of the mixing layer via the wavelet transform of the density field. The multifractal analysis is discussed.

4.2 Fractal dimension

In this section, we compute the fractal dimension of the interface between two fluids within the mixing layer induced by Rayleigh-Taylor instability. The temporal evolution of the interface is followed with a set of (initially aligned) particles. The heavy fluid is lying on top of the light fluid in a gravitational field. This numerical simulation of the Rayleigh-Taylor instability solves the Euler equations for each fluid, to which boundary conditions are imposed along the interface.

In our calculations ($\rho_1 = 0.1694\, kg/m^3$, $\rho_2 = 1.6\, kg/m^3$, and the Atwood number is equal to 0.81, see fig.3) between the time $t = 2.4430$ ms and the time $t = 3.0373$ ms the fractal dimension takes values between 1.73 to 1.69, for a large range of scales [1].

From these simulations, one may want to obtain average values for the mixture properties. We address here the problem of the effective opacity of the medium. Vanderhaegen [2] starts with the probability to find in the flow a scale x where the flow is homogeneous and considered a random medium constituted of spherical grains. For the species A and B, the distribution function of the chord X_i is Q_i $(i = A, B)$, the mean chord length is l_i, and the opacity is σ_i. The species A and B are weighted respectively by the probabilities p_A and p_B. Vanderhaegen derived an effective opacity σ_{eff} of the media by the following formulas

$$\begin{cases} \frac{1}{\sigma_{eff}} = \bar{l} - \frac{(\sigma_A - \sigma_B)^2}{\sigma_A \sigma_B (l_A + l_B)(\frac{\sigma_A}{q_B} + \frac{\sigma_B}{q_A} - \sigma_A \sigma_B)}, \\ q_i = \int_0^{+\infty} Q_i(x)\ e^{-\sigma_i x}\ dx, \\ \bar{l} = \frac{p_A}{\sigma_A} + \frac{p_B}{\sigma_B}\ . \end{cases} \tag{1}$$

In the following part, we take into account the Vanderhaegen 's method, but we will use a scaling law deduced directly from geometrical characteristics of the interface. Let us intersect the mixing layer between two materials A and B with a random line. We can deduce D from the two-dimensional fractal dimension ${D_f}^{(2D)}$ of the interface by [3] ${D_f}^{(2D)} = D + 1$. Let us note l_c a characteristic scale of the problem. We get the probability dQ [4] : $dQ(x) = (1 - D)(\frac{l_c}{x})^D \frac{dx}{l_c}$.

For sake of simplicity, and in the absence of any relevant information, we weight the species A and B by p_A and p_B, with $p_A = p_B = \frac{1}{2}$, and therefore $\bar{l} = \frac{1}{2}\,(\frac{1}{\sigma_A} + \frac{1}{\sigma_B})$. If we consider, after a certain time, the interface as a homogeneous fractal, we can simplify $Q_A = Q_B = Q$ which implies $l_A = l_B = l$. Therefore l is given by :

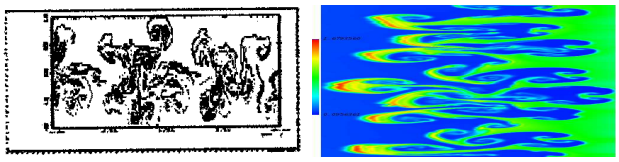

Figure 3: Marker particles initially located along the interface and considered at $t = 2.4430$ ms (left). Density field at $t = 1.9911$ ms (right).

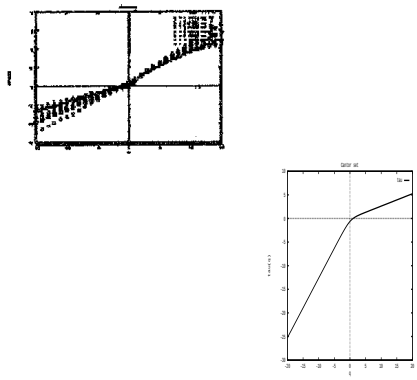

Figure 4: $\tau(q)$ for the Rayleigh-Taylor instability (left) and for the dissymmetric triadic Cantor set (right).

$l = l_c \frac{1-D}{(2-D)}$ and :

$$q_i = \frac{1 - e^{-\sigma_i l_c}}{\sigma_i} - {l_c}^{D-1} \int_0^{l_c} x^{1-D}\, e^{-\sigma_i\, x}\, dx\ . \tag{2}$$

To conclude, we can compute σ_{eff} by (1), but using now (2).

4.3 Wavelet Transform (WT)

In first section we modeled the inter-fluids interface with a homogeneous fractal set.In the following part, we keep a two-dimensional point of view. The multifractal analysis is made via the two-dimensional WT. The definition of the two-dimensional WT is :

$$\begin{aligned} T_\psi[f](b_1, b_2, a) &= \int\int_{R^2} f(x,y)\ \bar{\psi}_{a,b_1,b_2}(x,y)\ dx\ dy, \\ \psi_{a,b_1,b_2}(x,y) &= \tfrac{1}{a^2}\ \psi\ \left(\tfrac{x-b_1}{a}, \tfrac{y-b_2}{a}\right)\ , \end{aligned}$$

where b_1, b_2 are the position parameters ($b_1,\ b_2 \in R$) and a the scale parameter ($a > 0$). In this work, ψ is the Laplacian of a Gaussian function.

We study the density field computed by a numerical simulation of the Rayleigh-Taylor instability which solves the Euler two-fluids equations (3). We use a 1024×1024 grid. To interpret the singularities of the density field we plot the moments $M_q(\rho) = \int\int_{R^2} |T_\psi(\rho)|^q$ as functions of the scale parameter a, because of the following relation : $\int\int_{R^2} |T_\psi(\rho)|^q \sim a^{\tau(q)}$, with $\tau(q) = (q-1)D_q$. The generalized dimensions D_q describe the degree of inhomogeneity of a fractal set.

Let us note the similarity between our result and the function $\tau(q)$ of the dissymmetric triadic Cantor set (figure (4)) [4].

4.4 Conclusions

For the Rayleigh-Taylor instability, the measure of the fractal dimension of the interface can help to describe the mixing morphology. The fractal dimension is a global quantity, however we have been able to compute an effective opacity of the random medium via the fractal dimension.

The multifractal approach can be a useful analysis to describe the evolution of the small scales structures in the case of the Rayleigh-Taylor instability. In fact, in our case the density field can be considered as a singular measure. The modeling approach adopted here is based on the assumption that the geometry of the mixing layer may be described as a fractal or a multifractal set. The results obtained in the last section tend to confirm it. In fact, this study was done for a significant time scale.

References

[1] S. Mimouni, G. Laval, B. Scheurer, "Fractal Interface", EUROTHERM Seminar 39, NANTES, (1994).

[2] D. Vanderhaegen, J. Quant, Spectrosc. Radiat. Transfer, vol. 39, 4, 333–337 (1988).

[3] J.M. Marstrand, Proceedings of the London Mathematical Society (3), **4**, section 6, 257–302 (1954).

[4] S. Mimouni, G. Laval, B. Scheurer, S. Jaffard, "Morphology of the mixing layer in the Rayleigh-Taylor instability", Lecture Notes in Physics, Springer-Verlag, (1995).

[5] Lesieur M. 1990 *Turbulence in Fluids* Second revised edition, Kluwer Academic Publishers.

[6] Loreaux, Ph. 1995 Simulation numérique d'instabilités de mélange sur calculateurs massivement parallèles et schémas numériques d'ordre élevé, PhD thesis, Université Paris VI.

[7] Ducros, F., Comte, P., & Lesieur, M., 1995 Large-eddy simulation of a Spatially Weakly Compressible Boundary Layer over an adiabatic flat plate, to appear in Int. J. of Heat and Fluid Flow.

[8] Youngs, D., L. 1991 Three-dimensional numerical simulation of turbulent mixing by Rayleigh-Taylor instability *Phys. Fluids*, **A**, **3**, pp. 1312-1320.

[9] D. Besnard et. al., 1990 Spectral Transport Model of Turbulence. *Los Alamos National Laboratory Report, LA-11821-MS.*